EurJIC European Journal of Inorganic Chemistry

ChemPubSoc Europe

FULL PAPER

DOI:10.1002/ejic.201501092

Effect of Halopyridine Guest Molecules on the Structure and Superconducting Properties of β′′-[Bis(ethylenedithio)-tetrathiafulvalene]$_4$(H_3O)[$Fe(C_2O_4)_3$]·Guest Crystals

Tatiana G. Prokhorova,*[a] Lev I. Buravov,[a] Eduard B. Yagubskii,*[a] Leokadiya V. Zorina,*[b] Sergey V. Simonov,[b,c] Vladimir N. Zverev,[b,c] Rimma P. Shibaeva,[b] and Enric Canadell[d]

Keywords: Molecular conductors / Superconductors / Sulfur heterocycles / Solvent effects / Radical ions

Four new superconducting and metallic salts of the family of organic molecular conductors (BEDT-TTF)$_4$A^I[$Fe^{III}(C_2O_4)_3$]G [A = H_3O^+; G = 2-chloropyridine (**1**), 2-bromopyridine (**2**), 3-chloropyridine (**3**), and 3-bromopyridine (**4**); BEDT-TTF = bis(ethylenedithio)tetrathiafulvalene] have been prepared, and their crystal structures, electronic structures, transport properties, and magnetotransport properties have been studied. All of the crystals obtained belong to the monoclinic group of the family with β′′-type packing of the conducting BEDT-TTF layers. Crystals **1** and **2** are superconductors with T_c = 2.4–4.0 and 4.3 K, respectively, and possess structural phase transitions from monoclinic to triclinic symmetry at temperatures of 190–215 K, whereas **3** and **4** retain monoclinic symmetry at 90–300 K and do not show a superconducting transition above 0.5 K. Shubnikov–de Haas (SdH) oscillations were found in crystals of **1**, **2**, and **4**. The structures and conducting properties of **1**–**4** are compared with those of the known monoclinic phases of the family containing Fe^{III} ions and different monohalobenzenes and pyridine as "guest" solvent molecules (G).

Introduction

Molecular (super)conductors based on radical cation salts of the organic donor bis(ethylenedithio)tetrathiafulvalene (BEDT-TTF) have layered structures, in which the conducting layers of BEDT-TTF alternate with layers of insulating charge-compensating anions. The anions do not directly participate in conductivity, but their nature, shape, and size influence the structure of the cationic layers and, hence, the conductivity of the crystals. The largest group in this class of compounds is the family of BEDT-TTF salts with magnetic and nonmagnetic tris(oxalato)metallate anions (BEDT-TTF)$_4$A^I[$M^{III}(C_2O_4)_3$]G (A = K^+, NH_4^+, Rb^+, H_3O^+; M = Fe, Cr, Mn, Ru, Ga, Al, Co; G = "guest" solvent).[1–20] Crystals of this family possess a great diversity of conducting properties (from semiconducting to metallic and superconducting). A distinguishing feature of this anionic subsystem is the honeycomb-like architecture of the two-dimensional anionic layers: the M^{III} and A^I cations linked by oxalate bridges alternate at vertexes of the hexagonal network and form the hexagonal cavities, which are able to incorporate neutral solvent molecules G.

The components A, M, and G have different influences on the symmetry and properties of the crystals. The nature of the singly charged cation A^+ affects the properties of the crystals weakly, whereas the variation of M (with fixed A and G) leads to a noticeable change of conducting properties, in particular, the superconducting transition temperature (T_c). However, the "guest" solvent G plays the most important role: the symmetry of the crystals and the packing type of the BEDT-TTF layers are determined by G.

There are four groups of crystals in the (BEDT-TTF)$_4$A[$M(C_2O_4)_3$]G family: orthorhombic crystals with the "pseudo-κ" packing type of the BEDT-TTF layers,[1,6,13] monoclinic crystals with the β′′ packing type,[1–9,12,17,18] and triclinic ones with alternating α and β′′[10,11] or α and "pseudo-κ" layers.[13,14,20]

The orthorhombic group of the crystals contains some semiconductors (M^{III} = Fe, Cr, Co, Al; A = K^+, NH_4^+, H_3O^+; G = PhCN and its mixtures with $PhNO_2$ or 1,2-$C_6H_4Cl_2$). These crystals grow in "dry" solvents and also together with monoclinic crystals in the presence of traces of water.

[a] Institute of Problems of Chemical Physics, Russian Academy of Sciences,
142432 Chernogolovka, MD, Russia
E-mail: prokh@icp.ac.ru
yagubski@icp.ac.ru
http://www.icp.ac.ru
[b] Institute of Solid State Physics, Russian Academy of Sciences,
142432 Chernogolovka, MD, Russia
E-mail: zorina@issp.ac.ru
[c] Moscow Institute of Physics and Technology,
Dolgoprudny, Moscow Region, Russia
[d] Institut de Ciència de Materials de Barcelona, ICMAB-CSIC,
Campus de la UAB, 08193 Bellaterra, Spain

Supporting information for this article is available on the WWW under http://dx.doi.org/10.1002/ejic.201501092.

The triclinic salts with two different conducting layers were obtained with large, asymmetric guest solvent molecules [G = $PhCOCH_3$, $PhCOH(H)CH_3$, $(CH_3)_2NCHO$, $PhN(CH_3)CHO$, $PhCH_2CN$, 1,2-$C_6H_4Br_2$]. The formation of different conducting layers in these crystals is a result of an inequivalent arrangement of the large solvent molecules with respect to neighboring donor layers. The α–β′′ salts are semiconductors or exhibit metal–insulator transitions at low temperatures, whereas the α-pseudo-κ salts are metallic.

The large group of monoclinic crystals with the β′′ packing of the BEDT-TTF radical cations is the most interesting among the salts of this family. In particular, all of the superconducting crystals belong to this group. The monoclinic phases are formed if G is PhX (X = CN, NO_2, Cl, Br, F, I), C_3H_7NO (*N*,*N*-dimethylformamide), 1,2-$C_6H_4Cl_2$, C_5H_5N, CH_2Cl_2, as well as mixtures of PhCN with PhF, PhCl, PhBr, 1,2-$C_6H_4Cl_2$, $PhNO_2$, and C_5H_5N. The presence of small amounts of water in the reaction medium is a prerequisite for the formation of the monoclinic phases. A study of the monoclinic crystals showed that their structures and properties are determined not only by the size and the shape of the guest molecule G but also by its chemical nature. A structural phase transition from monoclinic *C*2/*c* to triclinic $P\bar{1}$ symmetry occurs at 180–230 K for several crystals in which G is PhF, PhCl, PhBr, or mixtures of these solvents with PhCN,[15,17] whereas phase transitions were not detected in the monoclinic crystals with the other solvents, including PhI. The structural phase transitions in several superconducting crystals (G = PhBr and PhCl/PhCN or PhF/PhCN mixtures) are accompanied by subtle changes in the ordering of the ethylene groups of BEDT-TTF, the consequences of which are phase transitions of these crystals from metallic to mixed metallic/insulating states.[19] According to the theoretical considerations of Merino and McKenzie,[21] the existence of this state precedes the appearance of superconductivity in crystals of organic conductors with a quarter-filled conduction band. To get additional information about the family of crystals containing halogenated solvents, we first used different monohalopyridines $C_5H_4(Hal)N$ (Hal = Cl, Br) as guest solvents for the synthesis of new salts of the family. The use of monohalopyridines opens up new opportunities for further investigation of the influence of guest molecules on the conducting properties, as the halogen atom may be in different positions with respect to the nitrogen atom of the pyridine ring. We report on the synthesis, structures, transport properties, and magnetotransport properties of four new radical cation salts β′′-$(BEDT\text{-}TTF)_4H_3O[Fe^{III}(C_2O_4)_3]G$ [G = 2-chloropyridine (2-C_5H_4ClN), **1**; 3-chloropyridine (3-C_5H_4ClN), **2**; 2-bromopyridine (2-C_5H_4BrN), **3**; and 3-bromopyridine (3-C_5H_4BrN), **4**].

Results and Discussion

Synthesis

Previously,[13] we showed that the addition of 96% ethanol and 1,2,4-trichlorobenzene (1,2,4-$C_6H_3Cl_3$) or 1,3-dibromobenzene (1,3-$C_6H_4Br_2$) to the reaction medium promotes the formation of monoclinic crystals of this family. The 1,2,4-$C_6H_3Cl_3$ and 1,3-$C_6H_4Br_2$ molecules are not involved in the composition of the crystals formed. Nevertheless, they play an important role in the electrochemical synthesis, as the reproducibility and selectivity of the syntheses and the quality of the crystals increase noticeably. In the present work, we used the "pure" solvents G and also different mixtures of G with 1,2,4-$C_6H_3Cl_3$, 96% ethanol, or both. The composition of the reaction medium affects the morphology of the growing crystals with monohalopyridine solvents. The use of "pure" 2-C_5H_4ClN or 2-C_5H_4BrN allowed us to obtain only very thin and fragile platelike crystals, whereas the use of mixtures of these solvents with ethanol and 1,2,4-$C_6H_3Cl_3$ led to formation of thick plates or hexagonal prisms, depending on the conditions of synthesis (crystals **1** and **2**). Unlike the salts with G = 2-$C_5H_4(Hal)N$, to synthesize crystals with G = 3-$C_5H_4(Hal)N$, the addition of 1,2,4-$C_6H_3Cl_3$ was not required; good-quality crystals of **3** and **4** were obtained from "pure" 3-C_5H_4ClN or a mixture of 3-C_5H_4BrN with ethanol, respectively. The obtained salts **1**–**4** are listed in Table 1.

Table 1. The new β′′-$(BEDT\text{-}TTF)_4(H_3O)[Fe(C_2O_4)_3]G$ salts and their properties.

Salt	G	Structural properties	Conducting properties
1	2-C_5H_4ClN	*C*2/*c* to $P\bar{1}$ transition at 215 K	superconducting, T_c = 2.4–4.0 K
2	2-C_5H_4BrN	*C*2/*c* to $P\bar{1}$ transition at 190 K	superconducting, T_c = 4.3 K
3	3-C_5H_4ClN	no structural transition	metallic above 0.5 K
4	3-C_5H_4BrN	no structural transition	metallic above 0.5 K

Crystal Structures

All of the studied crystals with monohalopyridine solvents have monoclinic structures with *C*2/*c* symmetry at room temperature, like the majority of the known crystals of the $(BEDT\text{-}TTF)_4A^I[M^{III}(C_2O_4)_3]G$ family. However, a low-temperature X-ray diffraction study showed an essential difference in the temperature behavior of the compounds. Crystals of **1** and **2** undergo structural phase transitions from monoclinic to triclinic symmetry at temperatures of 190 and 215 K (Table 1), respectively, whereas crystals **3** and **4** retain monoclinic symmetry in the whole temperature range of the X-ray diffraction experiments (90–300 K). The only reason for this structural distinction is the incorporation of different solvent isomers into the anion layer. Crystals **1** and **2** incorporate 2-halopyridine solvents, whereas **3** and **4** contain 3-halo-substituted ones. Here, a detailed comparison of the room- and low-temperature crystal structures is made for crystals **2** and **4** with 2-C_5H_4BrN and 3-C_5H_4BrN as guest molecules, respectively.

The asymmetric unit of the room-temperature monoclinic lattice includes two independent BEDT-TTF (A and B) molecules in general positions, half an $[Fe(C_2O_4)_3]^{3-}$ anion on a twofold axis, a solvent molecule, and an H_3O^+

cation in half-occupied general positions near a twofold axis.

The structure consists of conducting radical cation layers with β′′-type BEDT-TTF packing separated along *c* by complex anion layers $\{(H_3O)^+[Fe(C_2O_4)_3]^{3-}(C_5H_4BrN)\}^{2-}$ (Figure 1, a). The charge state of the two BEDT-TTF moieties is 0.5^+ according to the salt composition and the bond-length distribution in the TTF core [central C=C double bonds in A and B are 1.366(3) and 1.365(3) Å in **2** and 1.364(3) and 1.370(3) Å in **4**]. Both terminal ethylene groups of the radical cation B are disordered between two sites (with 0.70/0.30 occupancies in **2** and 0.65/0.35, 0.67/0.33 occupancies for the two BEDT-TTF ends in **4**), whereas A is fully ordered at room temperature. The latter is typical for all known β′′ crystals of the $(BEDT\text{-}TTF)_4A^I[M^{III}(C_2O_4)_3]G$ family.

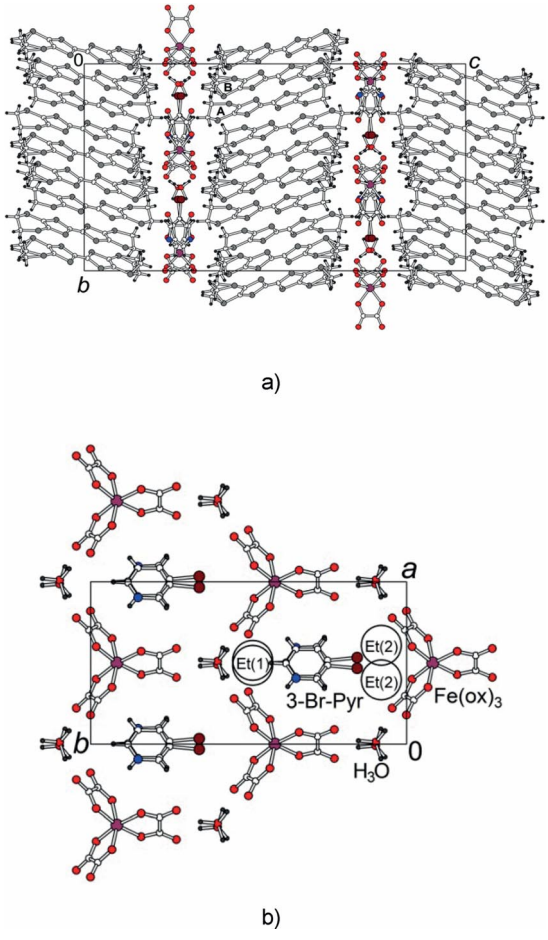

Figure 1. Monoclinic structure of **4** at room temperature: (a) view of the structure along *a* and (b) projection of the anion layer along *c* [the large circles mark the positions of the disordered terminal ethylene groups Et(1) and Et(2) of the disordered donor B situated above and below the plane of the anion layer].

Within the anion layer, the Fe^{3+} and H_3O^+ cations are connected by oxalato bridges to form a honeycomb-like network with solvent molecules incorporated inside the hexagonal cavities (Figure 1, b). The hexagonal units of the layers in the structures of **2** and **4** are represented in Figure 2 (a and b), respectively. Some differences between the solvent positions in these structures are already apparent at room temperature. The $2\text{-}C_5H_4BrN$ molecule in **2** and the $3\text{-}C_5H_4BrN$ molecule in **4** are shifted along the twofold axis of the monoclinic lattice in opposite directions, as shown by the red arrows in Figure 2. As a result, the Br···Fe distance to the nearest anion is shorter by 0.25 Å in **2** [4.562(1) Å] than in **4** [4.801(1) Å] and, correspondingly, the (C)H···O distance between the H_3O ion and the hydrogen atom attached to the C atom at the *para* position with respect to the Br atom is longer in **2** (3.65 Å) than in **4** (3.40 Å). Note that the solvent and H_3O^+ ions are disordered about a twofold axis. For easier comparison, all listed measurements are made between the centroids of the Br, H, or O pairs lying exactly on the twofold axis. The mutual positions of the anionic oxalato ligands are also diverse in **2** and **4**. This is manifested by a difference in the dihedral angles between the two oxalato ligands ox(1) and ox(1)′ related by a twofold axis [84.61(6) and 86.81(5)° in **2** and **4**, respectively] and between the third oxalato ligand ox(2) and the *ab* plane of the anion layer [57.93(3) and 55.07(3)° in **2** and **4**, respectively]. The twist of the oxalato ligands leads to shorter $O_{ox}\cdots O_{ox}$ intracavity distances in **4** in comparison with those in **2** (Figure 1). To fit the different surroundings, the dihedral angle between the pyridine plane and the cavity plane increases from 33.7(3)° in **2** to 36.4(4)° in **4**.

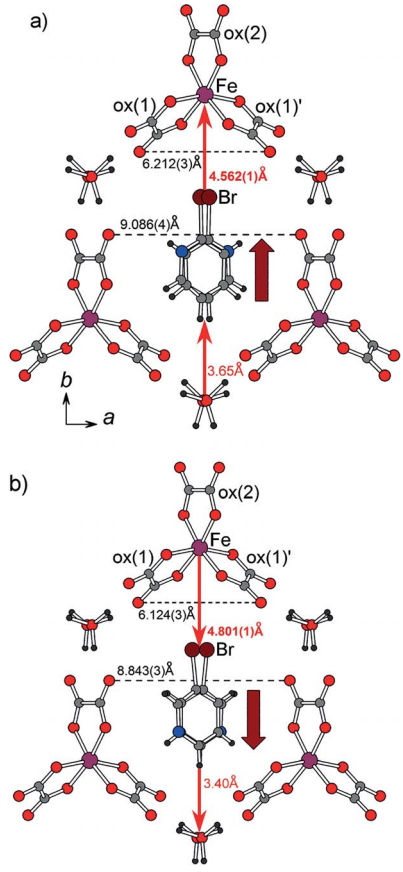

Figure 2. Hexagonal units of the anion layers in (a) **2** and (b) **4** at room temperature.

The structural transition in **2** occurs at 190 K. Below this temperature, additional diffraction reflections reveal the disappearance of the systematic absences of the monoclinic *C*2/*c* lattice and the reduction of symmetry to the triclinic $P\bar{1}$. A similar phase transition was described in detail before for several crystals of the family with monohalobenzene solvents (PhF, PhCl, PhBr or their mixtures with PhCN, in which the amount of PhCN is less than 40%).[15,17] In the $P\bar{1}$ structure of **2**, four independent donors form two inequivalent conducting layers: the T1 layer is built of A1 and B1 radical cations, and the T2 layer is built of A2 and B2 radical cations (Figure S1 in the Supporting Information). A partial ordering occurs in the donors B1 and B2, which were disordered at room temperature. At 120 K, one terminal ethylene group of each donor becomes fully ordered, whereas two sites are found for the second one with 0.52/0.48 and 0.67/0.33 probabilities for B1 and B2, respectively. In the anion layer of the triclinic phase, the noticeable shifts of pyridine ring of the solvent molecule to the BEDT-TTF layer T1 and the H_3O^+ ions to the layer T2 are observed (shown by the arrows in Figure S1). At the same time, there is no significant difference between the BEDT-TTF charge in the two layers: the central C=C bond lengths in the TTF part are 1.365(6) Å for A1/B1 and 1.371(6) and 1.376(6) Å for A2 and B2, respectively.

Crystal **4** does not undergo a structural transition as the temperature decreases and retains the monoclinic structure at 100 K. The disorder of the solvent and H_3O^+ ions, which is shown for the room-temperature state in Figure 2 (b), also persists at 100 K. In BEDT-TTF B, one of the ethylene ends, which forms short contacts with a disordered Br atom, remains disordered between two sites with occupancies of 0.67/0.33 (which are close to the values of 0.65/0.35 at room temperature), whereas the second one still shows 10% of the minor orientation at 100 K.

The same differences between the structures of the anion layer in **2** and **4** as those shown in Figure 2 for room temperature are observed in the low-temperature state: a diverse shift of the solvent molecule along the twofold axis and a corresponding twist of the oxalato ligands leads to distinct $O_{ox}\cdots O_{ox}$ distances inside the cavity. The reason can be found in the molecular structures of two solvents (Figure 3). The half of the pyridine ring opposite the Br atom is broader in 2-C_5H_4BrN as it involves three CH groups instead of two CH groups and one N atom in 3-C_5H_4BrN. Therefore, the 2-C_5H_4BrN molecule should be moved along the C–Br vector to better fit the cavity and avoid too short C–H$\cdots O_{ox}$ contacts. It is worth noting that we change the orientation of N vertex of the pyridine ring in the cavity of the anion layer by using halopyridines, as the N atom of the unsubstituted pyridine molecule lies on a twofold axis and is oriented to the nearest H_3O^+ cation (i.e., directed to the bottom vertex of the cavity in Figure 2). Note also that the monoclinic to triclinic structural transition was not found above 90 K for the crystals with G = C_5H_5N.[3]

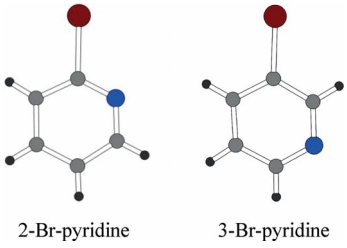

Figure 3. Br-substituted pyridine molecules: (left) 2-bromopyridine and (right) 3-bromopyridine.

The structures with G = 2-C_5H_4ClN (**1**) and 3-C_5H_4ClN (**3**) demonstrate exactly the same features as salts **2** and **4** with C_5H_4BrN. The Cl$\cdots$Fe distances to the nearest anion in the monoclinic state are 4.583(1) Å for **1** (at 295 K) and 4.874(1) Å for **3** (at 120 K). The *C*2/*c* to $P\bar{1}$ transition of **1** occurs at 215 K.

It is of interest to compare structures with monohalopyridine and monohalobenzene molecules as the guest solvent. As the halobenzene molecules have three CH groups in the half of the benzene ring opposite the halogen atom, as in 2-C_5H_4(Hal)N, it is not surprising that the Hal$\cdots$Fe distances for G = 2-C_5H_4(Hal)N and Ph(Hal) are quite similar, namely, 4.562 Å for 2-C_5H_4BrN, 4.584 Å for PhBr, 4.583 Å for 2-C_5H_4ClN, and 4.651 Å for PhCl, whereas remarkably larger Hal$\cdots$Fe distances of more than 4.8 Å are found for G = 3-C_5H_4(Hal)N. Therefore, in the structures of **3** and **4** with G = 3-C_5H_4(Hal)N, there is more free space in the cavity near the halogen atom. This is important for the structural disorder in these salts. The terminal ethylene groups of the independent BEDT-TTF radical cation that is always disordered at room temperature (molecule B) are located above and below the free volume of the cavity near the disordered solvent molecule (Figure 1, b), whereas the ordered groups of the other BEDT-TTF (molecule A) are closer to the ordered anions. In the triclinic structures of **1** and **2**, disordered donors B become partially ordered: full ordering is observed at 120 K for the Et(1) group of the B1 molecule and the Et(2) group of the B2 molecule [see Figure 1 (b) for Et(1) and Et(2) labeling]. In **3** and **4**, the B donor remains disordered upon cooling, but the occupancy of the disordered Et(1) site changes from 0.67/0.33 at 295 K to 0.90/0.10 at 120 K in **4** (0.83/0.17 at 120 K in **3**), whereas that of Et(2), which forms hydrogen bonds to the disordered halogen atom, persists at the same level. The conservation of positional disorder within the radical cation layer at low temperature impedes superconductivity in BEDT-TTF conductors.

Transport and Magnetotransport Properties

The temperature dependences of the normalized resistance of the samples with different composition are shown in Figure 4. The values of the room-temperature resistivity of the samples are presented in Table 2. All of the samples had metallic-like temperature dependences in the whole temperature range, except for **3**, the resistance of which increased as the temperature decreased below 40 K. Nevertheless, this sample is still a good conductor down to the

lowest temperature of 0.5 K. As seen from Figure 4, **1** and **2** are superconductors, and their onset critical temperatures T_c are presented in Table 1. Interestingly, the room-temperature out-of-plane resistivities of the superconducting samples (**1** and **2**) are greater than those of the non-superconducting samples, which probably indicates that superconductivity occurs preferentially in the systems with higher anisotropy, that is, in the more two-dimensional systems.

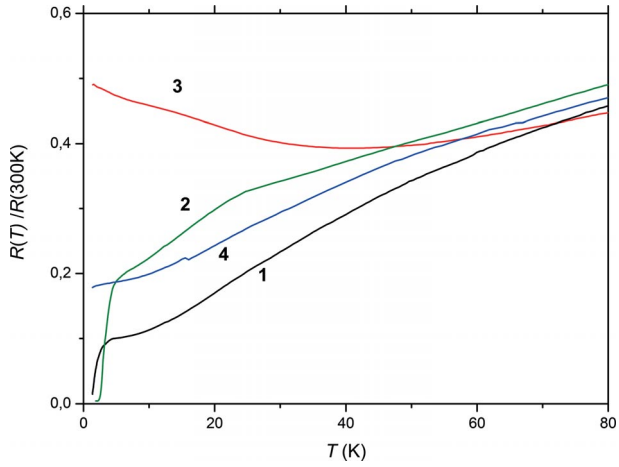

Figure 4. The temperature dependences of the normalized resistance $R(T)/R$ (300 K) of **1**–**4**.

Table 2. The results of the transport and SdH oscillation measurements of **1**–**4**.

Salt	$\rho_\perp$ (300 K), [Ω cm]	Fourier frequency of SdH oscillations [T]	m^*/m_0	S/S_{BZ}[a]
1	260	388	1.43	9.59%
		293	1.48	7.24%
2	190	278	1.3	6.88%
3	20	–	–	–
4	10.5	287	1.71	7.2%

[a] S_{BZ} was calculated for the triclinic cell setting.

We have studied the magnetotransport properties of our samples at low temperatures and have observed the Shubnikov–de Haas (SdH) oscillations of the $R(B)$ dependences. Unfortunately, we did not observe the oscillation of **3**, probably because of the comparatively low quality of this sample. This assumption was confirmed by the $R(T)$ dependence of this sample at low temperature, which is characteristic for a "bad" metal (see Figure 4). The SdH oscillations at 0.5 K as well as their Fourier spectra are shown in Figure 5 (a and b) for **1** and **2**. The Fourier spectra were obtained by the fast Fourier transformation of the oscillatory component of the resistance $(R - R_{pol})/R_{pol}$, in which R_{pol} is a polynomial fit of the $R(B)$ dependence over the field range 10–17 T.

One can see that the SdH oscillations of **1** are characterized by the presence of two fundamental frequencies, which is in contrast to the results obtained for the other samples, for which the oscillations contain only one dominant frequency. As can be seen in Table 2, these characteristic frequencies are close to the lowest one observed for **1**.

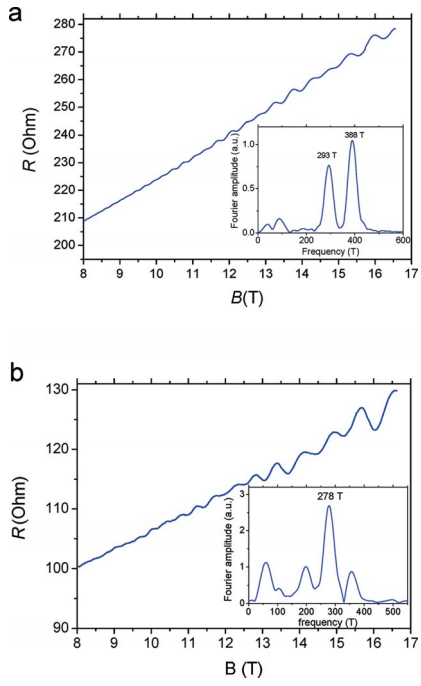

Figure 5. The SdH oscillations of the magnetoresistance of (a) **1** and (b) **2** at T = 0.5 K. The Fourier spectra of the oscillations are shown in the insets.

For **4**, the Fourier spectrum of the oscillations looks very similar to that of **2** but is characterized by a slightly different dominant frequency. From the temperature dependence of the Fourier amplitude A, the values of the electron cyclotron mass m^*/m_0 (m_0 is the free electron mass) corresponding to the observed frequencies were obtained through standard Lifshitz–Kosevich analysis.[22]

This procedure is illustrated in Figure 6, in which the so-called "mass plot" is presented as an example for both frequencies observed for **1** (see Figure 5, a). The results of the transport and SdH oscillation measurements of the samples are summarized in Table 2, which contains only the data concerning the dominant components of the Fourier spectra. The low-amplitude components could be either artefacts (at low frequencies) caused by the polynomial subtrac-

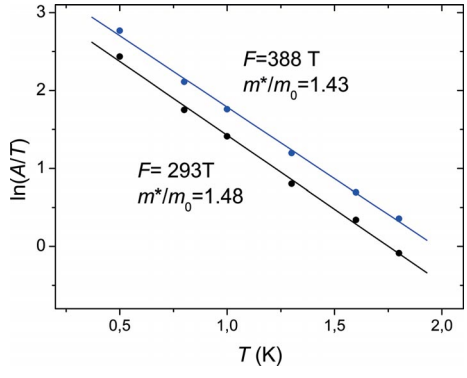

Figure 6. The mass plot for two components of the Fourier spectrum of the SdH oscillations of **1**. A is the normalized amplitude of the SdH oscillations, obtained by Fourier analysis.

tion or components with a combination of frequencies as a result of frequency mixing. In the right column of Table 2, the areas of the extreme cross-section of the Fermi surface S/S_{BZ} in the *ab* plane, calculated from the observed SdH oscillation frequencies, are presented (S_{BZ} is the area of the Brillouin zone cross-section). The S_{BZ} values were calculated from our X-ray data obtained at 100–120 K (the triclinic cell setting was used for all crystals to enable easier comparison).

Electronic Band Structure

Calculations for the different donor layers (T1 and T2 in Figure S1) of the triclinic structure of superconducting salt **2** and the monoclinic structure of non-superconducting salt **4** were performed exactly as in our previous study[15] of β′′-(BEDT-TTF)$_4$H$_3$O[Fe(C$_2$O$_4$)$_3$]G [G = (PhCN)$_{0.35}$(PhCl)$_{0.65}$] to enable the direct comparison of the results. As shown in Figure 7 for one of the two different donor layers of **2** in the triclinic structure, every donor layer of these salts contains two different donors noted as A and B, and the repeat unit contains four donors. There are eight different donor–donor interactions: three along the stacks (I to III), two along the step-chain direction (VII and VIII), and finally three lateral π-type interactions (IV to VI). The calculated $\beta_{HOMO-HOMO}$ (HOMO = highest occupied molecular orbital) interaction energies[23] for the eight donor–donor interactions of the two layers in the triclinic structure of **2** are reported in Table 3. These values clearly show that the differences in the strengths of the HOMO–HOMO interactions are small. Only three of the interactions, that is, III (B–B), VII (A–B), and VIII (A–B) in one of the two layers, show noticeable variations. Interactions VII and VIII along the step chains change in opposite directions, and their effects partially cancel. Such differences should not afford clear changes in the electronic structure of β′′ slabs such as the present ones. It is worth noting that these interactions are associated with σ-type S···S interactions of donor B, which exhibits different degrees of order in the two layers so that the small variations reflect the influence of the disorder of the terminal ethylenedithio groups on the HOMO–HOMO interactions. The calculated energies of the HOMO for the different donors in a layer are very similar and lie in a very narrow energy range of 0.03 eV. Consequently, neither the HOMO energies nor the HOMO–HOMO interactions differ enough to expect that there are important differences in the electronic structures of the two layers. Similar conclusions were reached for β′′-(BEDT-TTF)$_4$H$_3$O[Fe(C$_2$O$_4$)$_3$](PhCN)$_{0.35}$(PhCl)$_{0.65}$[15] for the difference between the layers of the triclinic phase and between those of the triclinic and monoclinic phases.

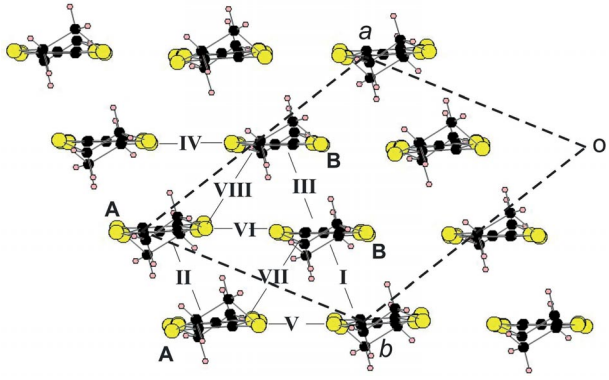

Figure 7. One of the two donor layers (layer T2) of **2** in the triclinic structure with the different donors (A and B) and donor–donor interactions (I to VIII) labeled.

Table 3. Calculated values of $|\beta_{HOMO-HOMO}|$ [eV] for the different donor···donor interactions in the two different β′′ layers of the triclinic structure of **2**.

Interaction	Layer T1[a]	Layer T2[b]
I (A–B)	0.2323	0.2220
II (A–A)	0.1274	0.1262
III (B–B)	0.1296	0.0913
IV (B–B)	0.1666	0.1526
V (A–A)	0.0913	0.0945
VI (A–B)	0.1530	0.1567
VII (A–B)	0.2449	0.2706
VIII (A–B)	0.3054	0.2866

[a] Layer T1 contains donors A1 and B1. [b] Layer T2 contains donors A2 and B2.

The calculated band structure and Fermi surface for layer T2 in the triclinic structure of **2** are shown in Figure 8 (a and b). The calculations for the monoclinic structure of **4** (Figures S2 and S3) and the two different layers of the

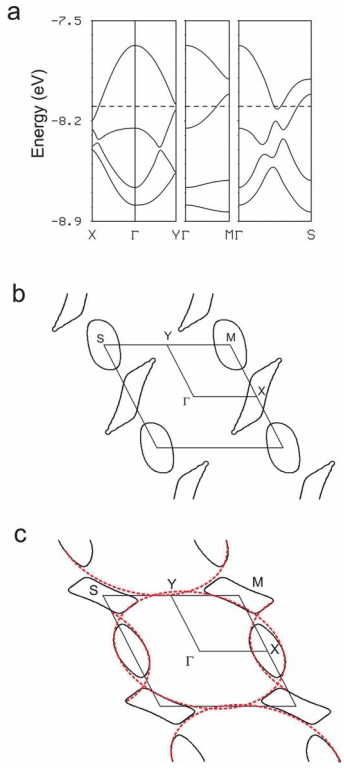

Figure 8. (a) Band structure calculated for layer T2 in the triclinic structure of **2**. The dashed line refers to the Fermi level. Γ = (0, 0), X = (*a**/2, 0), Y = (0, *b**/2), M = (*a**/2, *b**/2), and S = (–*a**/2, *b**/2). Fermi surface calculated for layers (b) T2 and (c) T1 of **2**. In (c), it is shown how these Fermi surfaces result from the hybridization of a series of ellipses with an area of 100% of the cross-section of the Brillouin zone.

triclinic structure of **2** (Figures 8 and S4) are very similar, as expected from previous results.[15] The only slight difference is in the detailed shape of one of the two components of the Fermi surface. Although layer T2 of the triclinic structure of **2** exhibits the shape shown in Figure 8 (b), those of layer T1 and the monoclinic structure of **4** exhibit the Fermi surface shown in Figure 8 (c), which has more rectangular-like electron pockets. These Fermi surfaces are made of closed electron and hole pockets with areas of 8.4 and 9.7% of the cross-section of the Brillouin zone for layers T1 and T2 of **2** and 8.4% for the single layer of **4**, respectively. These areas agree reasonably well with those derived from our magnetoresistance measurements (see Table 2).

As schematically shown in Figure 8 (c), these closed pockets result from the hybridization of superposing ellipses with an area of 100% of the cross-section of the Brillouin zone. The subtle change of the electron pockets from the shape shown around X in Figure 8 (b) to that shown around M (and S) in Figure 8 (c) only depends on how these ellipses actually superpose. However, the differences between the two Fermi surfaces are not significant enough to lead to strong differences in the physical properties. These Fermi surfaces do not exhibit any nesting properties; therefore, it is expected that the metallic state should be stable until very low temperatures.

Let us mention that the Fermi surfaces of Figure 8 (b and c) are almost identical to those of layers T2 and T1 of β′′-(BEDT-TTF)$_4$H$_3$O[Fe(C$_2$O$_4$)$_3$](PhCN)$_{0.35}$(PhCl)$_{0.65}$,[15] respectively. However, in that case, the area of the pockets in the two different layers was calculated to be practically identical. These results make it clear that it is possible to observe either two or just one SdH oscillation frequency, depending on the difference between the areas of the closed pockets of the Fermi surfaces associated with each layer, because of the occurrence of two slightly different layers in the triclinic structures of these salts. To more thoroughly consider this point, we also calculated the Fermi surfaces of **1** with G = 2-C$_5$H$_4$ClN (Figure S5). The area of the closed pockets associated with layers T1 and T2 of this salt were calculated to be 8.6 and 10.3% of the cross-section of the Brillouin zone and, thus, confirmed our expectations and the experimental observation of two different SdH frequencies (see Table 2). The apparent contradiction between the computational and experimental results for **2** (different calculated area of closed pockets for T1 and T2 layers but only one main SdH frequency observed) could have two different origins: (1) the difference between the closed pockets of the T1 and T2 layers of **2** is somewhat exaggerated in the present calculations and the pockets should be more similar, as for β′′-(BEDT-TTF)$_4$H$_3$O[Fe(C$_2$O$_4$)$_3$](PhCN)$_{0.35}$(PhCl)$_{0.65}$; (2) for some still unknown reason, one of the two SdH frequencies is difficult to observe in the present samples. This point certainly warrants further attention to clarify the interesting low-temperature behavior of these phases.

To further examine if there is some simple correlation for these salts between the structure at low temperature and superconductivity, we have calculated the densities of states at the Fermi level for the different layers of **2**, **4**, and β′′-(BEDT-TTF)$_4$H$_3$O[Fe(C$_2$O$_4$)$_3$](PhCN)$_{0.35}$(PhCl)$_{0.65}$. As shown in Table 4, when there is a transition from a monoclinic to triclinic structure, the value of $N(E_F)$ becomes somewhat different for the two layers. This subtle variation, which is most likely related to the different degree of disorder of one of the donors in the two layers, is thus the only change in the electronic structure caused by the transition. From the values in Table 4, it could be thought that the fact that $N(E_F)$ for the non-superconducting salt **4** is the smallest could be taken as an indication that there is a correlation between $N(E_F)$ and T_c. However, for the two superconducting salts, both the total values or those for the layer with the larger $N(E_F)$ (i.e., layer T2) change in the opposite way of the variation of T_c. Thus, there is not a correlation between T_c and $N(E_F)$, and we must conclude that the subtle variations in the electronic structure are probably not at the origin of the differences exhibited by these salts with respect to their superconductivity.

Table 4. Calculated values of the density of states at the Fermi level $N(E_F)$ [electrons/eV/unit cell] for the donor layers of β′′-(BEDT-TTF)$_4$H$_3$O[Fe(C$_2$O$_4$)$_3$]G salts.

	$N(E_F)$	Total $N(E_F)$
G: 2-C$_5$H$_4$BrN, **2** [T_c = 4.3 K]		
Layer T1 [a]	4.892	10.915
Layer T2 [b]	6.023	
G: (PhCN)$_{0.35}$(PhCl)$_{0.65}$ [T_c = 6 K]		
Layer T1 [a]	4.896	10.641
Layer T2 [b]	5.745	
G: 3-C$_5$H$_4$BrN, **4** (non-superconducting)		
Unique layer	5.216	10.432

[a] Layer T1 contains donors A1 and B1. [b] Layer T2 contains donors A2 and B2.

Conclusions

The monohalopyridines were used for the first time as guest molecules (G) in the synthesis of BEDT-TTF radical cation salts with tris(oxalato)metallate anions, and four new salts of the β′′-(BEDT-TTF)$_4$H$_3$O[Fe^{III}(C$_2$O$_4$)$_3$]·G family with G = 2-chloropyridine (**1**), 2-bromopyridine (**2**), 3-chloropyridine (**3**), and 3-bromopyridine (**4**) were obtained. The salts are isostructural to other members of the monoclinic group of this family (*C*2/*c* symmetry) with the β′′ packing motif of conducting BEDT-TTF layers separated along the *c* axis by complex anion layers {(H$_3$O)$^+$[Fe(C$_2$O$_4$)$_3$]$^{3-}$G}$^{2-}$, which contain guest solvent molecules (G) inside the hexagonal cavities of the honeycomb-like network. The incorporation of different monohalopyridine isomers into the anion layer affords crystals with different conducting and structural properties. The salts **1** and **2**, containing 2-chloro- and 2-bromopyridine, demonstrate structural transitions from the monoclinic to triclinic phase at 190 and 215 K and undergo superconducting transitions with T_c = 2.4–4.0 and

4.3 K, respectively. In contrast, **3** and **4**, containing 3-chloro- and 3-bromopyridine, keep the monoclinic symmetry in the whole temperature range of the X-ray diffraction experiments (90–300 K) and do not show a superconducting transition above 0.5 K. Thus, in spite of the equal volume and longitudinal size of the 2- and 3-halopyridine isomers, their use in the synthesis of the title family of salts produces monoclinic crystals with very different temperature dependences of the crystal structure and conductivity. The crystal structures of **1**–**4** show significant variations between the solvent position inside the hexagonal cavity for 2-C_5H_4(Hal)N and 3-C_5H_4(Hal)N solvents both at room and low temperature. As a result, the structures of **3** and **4** with G = 3-C_5H_4(Hal)N have more free space in the cavities near the halogen atoms in comparison with **1** and **2** with G = 2-C_5H_4(Hal)N. This determines different degrees of structural disorder in these salts upon cooling. Although radical cation B has similar disorder of both terminal ethylene groups of BEDT-TTF in **1**–**4** at room temperature, one of the ethylene groups in each of two independent BEDT-TTF radical cations (B1 and B2) in the superconducting crystals **1** and **2** become fully ordered in the triclinic phase at 120 K, whereas both ethylene ends of donor B remain disordered in the monoclinic phase at 100–120 K for the non-superconducting salts **3** and **4**.

The study of the electronic structures and magnetoresistance properties reveal that the Fermi surfaces in these salts are built from closed electron/hole pockets. Subtle variations in the electronic structures of the triclinic and monoclinic phases are found but they cannot be at the origin of the differences exhibited by these salts with respect to their superconductivity. The absence of superconductivity in the crystals of **3** and **4** is most likely associated with the higher degree of disorder in their structures at low temperatures. In contrast to the salts with 2-halopyridines, the β′′ salt with the parent pyridine as the "guest" molecule does not possess superconductivity because of the occurrence of a positional disorder in the cationic and anionic layers that persists at 90 K.[3] The salts with a low-temperature triclinic structure can exhibit either one or two different SdH oscillation frequencies, depending on how different the closed pockets of the Fermi surfaces associated with the two different layers of the structure are. The experimental observation of two different SdH frequencies for crystals of salt **1** agrees well with the Fermi surfaces calculated for two layers of the triclinic structure of **1**.

Experimental Section

Synthesis of Radical Cation Salts: BEDT-TTF, 1,2,4-$C_6H_3Cl_3$, 2-C_5H_4ClN, 3-C_5H_4ClN, 2-C_5H_4BrN, 3-C_5H_4BrN, and $(NH_4)_3$-$[Fe(C_2O_4)_3]\cdot 3H_2O$ were used as received (Aldrich); 18-crown-6 (Aldrich) was purified by recrystallization from acetonitrile and dried in vacuo at 30 °C with P_2O_5.

Electrocrystallization of the charge-transfer salts was performed in conventional two-compartment H-shaped cells with Pt wire electrodes at constant current and temperature (25 °C). BEDT-TTF, the supporting electrolyte, 18-crown-6, and a solvent (or a mixture of solvents) were placed in the cathode compartment of the cell. The obtained solution was distributed between the two compartments of the cell. The exact conditions for the synthesis of each salt are described below.

β′′-(BEDT-TTF)$_4$(H_3O)[$Fe(C_2O_4)_3$]·(2-C_5H_4ClN) (1): BEDT-TTF (17 mg), $[NH_4]_3[Fe(C_2O_4)_3]\cdot 3H_2O$ (170 mg), 18-crown-6 (170 mg), 1,2,4-$C_6H_3Cl_3$ (7 mL), 2-C_5H_4ClN (20 mL), 96% ethanol (3 mL); J = 0.9 μA. Crystals in the form of hexagonal prisms were collected from the anode after three weeks.

β′′-(BEDT-TTF)$_4$(H_3O)[$Fe(C_2O_4)_3$]·(2-C_5H_4BrN) (2): BEDT-TTF (15 mg), $[NH_4]_3[Fe(C_2O_4)_3]\cdot 3H_2O$ (100 mg), 18-crown-6 (200 mg), 1,2,4-$C_6H_3Cl_3$ (10 mL), 2-C_5H_4BrN (25 mL), 96% ethanol (2 mL); J = 0.75 μA. Crystals in the form of thick plates were collected from the anode after 17 d.

β′′-(BEDT-TTF)$_4$(H_3O)[$Fe(C_2O_4)_3$]·(3-C_5H_4ClN) (3): BEDT-TTF (15 mg), $[NH_4]_3[Fe(C_2O_4)_3]\cdot 3H_2O$ (150 mg), 18-crown-6 (300 mg), 3-C_5H_4ClN (20 mL); J = 0.9 μA. Crystals in the form of plates were collected from the anode after 13 d.

β′′-(BEDT-TTF)$_4$(H_3O)[$Fe(C_2O_4)_3$]·(3-C_5H_4BrN) (4): BEDT-TTF (15 mg), $[NH_4]_3[Fe(C_2O_4)_3]\cdot 3H_2O$ (150 mg), 18-crown-6 (300 mg), 3-C_5H_4BrN (20 mL), 96% ethanol (2 mL); J = 0.85 μA. A lot of crystals of very good quality in the form of thick plates were collected from the anode after 12 d.

Crystal Structure Determination: The single-crystal X-ray structural study was performed with an Oxford Diffraction Gemini-R diffractometer [Mo-K_α radiation, λ = 0.71073 Å, graphite monochromator, Atlas CCD detector] in the temperature range 300–90 K with a Cryojet nitrogen cooler. For the crystals of **1** and **2**, a structural phase transition from monoclinic to triclinic symmetry was found between 190 and 215 K, whereas crystals of **3** and **4** are monoclinic down to 90 K. The transition was detected through the disappearance of the systematic absences of the monoclinic phase in X-ray rotation images obtained at a cooling rate of 20 K/h with 3–5° steps. For all of the crystals, full data collections were performed at room temperature and 120 or 100 K by using ω-scanning. Data reduction with empirical absorption correction of experimental intensities (Scale3AbsPack program) was performed with the CrysAlisPro software.[24]

The structures were solved by direct methods followed by Fourier syntheses and refined by a full-matrix least-squares method by using the SHELX-97 programs[25] in an anisotropic approximation for all non-hydrogen atoms. The H atoms in BEDT-TTF and solvent molecules were placed in idealized positions and refined by using a riding model with U_{iso}(H) fixed at 1.2U_{eq}(C). The coordinates of the H atoms in the hydroxonium cations were found from difference electron density maps and refined with U_{iso}(H) = 1.5U_{eq}(O), and the O–H bond lengths were restrained to equal values with standard deviations of 0.01–0.02 Å (SADI instruction). Restraints with the SADI instruction were used also for the C–C and C–N bond lengths in the pyridine rings of the disordered solvent molecules in all the structures. In the triclinic phase, the crystals become twinned through a twofold rotation around the former monoclinic axis. The refined twin fractions are 0.239(1) for **1** and 0.173(1) for **2**. The unit-cell parameters and details of the data collection and structure refinement are collected in Table 5.

CCDC-1420510 (for **1** at 295 K), -1420511 (for **1** at 120 K), -1420512 (for **2** at 295 K), -1420513 (for **2** at 120 K), -1420514 (for **3**), -1420515 (for **4** at 295 K), and -1420516 (for **4** at 100 K) contain the supplementary crystallographic data for this paper. These data can be obtained free of charge from The Cambridge Crystallographic Data Centre via www.ccdc.cam.ac.uk/data_request/cif.

Table 5. Crystal structure and refinement data. X-ray diffraction experiments were performed with Mo-K_α radiation (λ = 0.71073 Å).

	1	**1**	**2**	**2**
Chemical formula	$C_{51}H_{39}ClFeNO_{13}S_{32}$	$C_{51}H_{39}ClFeNO_{13}S_{32}$	$C_{51}H_{39}BrFeNO_{13}S_{32}$	$C_{51}H_{39}BrFeNO_{13}S_{32}$
Formula weight	1991.05	1991.05	2035.51	2035.51
Temperature [K]	295	120	295	120
Cell setting	monoclinic	triclinic	monoclinic	triclinic
Space group, Z	$C2/c$, 4	$P\bar{1}$, 2	$C2/c$, 4	$P\bar{1}$, 2
a [Å]	10.3051(2)	10.2840(2)	10.3035(2)	10.2728(1)
b [Å]	19.9856(6)	11.1515(3)	20.0265(5)	11.1710(1)
c [Å]	35.3435(10)	35.1159(6)	35.448(1)	35.1921(5)
α [°]	90	87.657(2)	90	87.626(1)
β [°]	93.156(2)	86.324(2)	93.442(2)	86.064(1)
γ [°]	90	62.628(2)	90	62.728(1)
Cell volume [Å^3]	7268.1(3)	3568.6(1)	7301.2(4)	3580.93(8)
ρ [Mg/m^3]	1.820	1.853	1.852	1.888
μ [mm^{-1}]	1.224	1.247	1.729	1.763
Reflections collected/unique	16890/9521	43915/19048	22167/10046	48458/18000
R_{int}	0.0194	0.0292	0.0235	0.0225
$\theta_{max.}$ [°]	29.89	30.23	30.65	29.66
Parameters refined	528	991	528	957
Final R_1, wR_2 [$I>2\sigma(I)$]	0.0363, 0.0878	0.0803, 0.2210	0.0459, 0.1115	0.0508, 0.1248
Goodness-of-fit	1.005	1.019	1.007	1.005
	3	**4**	**4**	
Chemical formula	$C_{51}H_{39}ClFeNO_{13}S_{32}$	$C_{51}H_{39}BrFeNO_{13}S_{32}$	$C_{51}H_{39}BrFeNO_{13}S_{32}$	
Formula weight	1991.05	2035.51	2035.51	
Temperature [K]	120	295	100	
Cell setting	monoclinic	monoclinic	monoclinic	
Space group, Z	$C2/c$, 4	$C2/c$, 4	$C2/c$, 4	
a [Å]	10.2513(2)	10.2906(2)	10.2460(2)	
b [Å]	19.8295(3)	20.0328(5)	19.8214(3)	
c [Å]	34.9318(6)	35.3670(7)	35.034(1)	
α [°]	90	90	90	
β [°]	93.463(2)	93.051(2)	93.745(2)	
γ [°]	90	90	90	
Cell volume [Å^3]	7087.9(2)	7280.6(3)	7099.8(3)	
ρ [Mg/m^3]	1.866	1.857	1.904	
μ [mm^{-1}]	1.255	1.734	1.778	
Reflections collected/unique	9343	41196/10349	35265/10059	
R_{int}	0.0144	0.0222	0.0216	
$\theta_{max.}$ [°]	29.99	30.63	30.66	
Parameters refined	528	528	528	
Final R_1, wR_2 [$I>2\sigma(I)$]	0.0309, 0.0649	0.0403, 0.0916	0.0296, 0.0663	
Goodness-of-fit	1.027	1.010	1.007	

Conductivity and Magnetotransport Measurements: The temperature dependences of the electrical resistance of single crystals were measured by a four-probe technique with a lock-in detector at 20 Hz and alternating current J = 1 μA. Two contacts were attached to each of two opposite sample surfaces with conducting graphite paste. We measured the out-of-plane resistance $R_\perp$ with the current running perpendicular to the conducting layers. The magnetotransport measurements at low temperatures down to 0.5 K were performed in a cryostat with a superconducting solenoid, which generated a magnetic field of up to 17 T. In all magnetotransport measurements, the magnetic field B was directed along the c axis of the samples $B\|c$.

Electronic Band Structure Calculations: The tight-binding band structure calculations[26] were of the extended Hückel type, and a modified Wolfsberg–Helmholtz formula was used to calculate the nondiagonal $H_{\mu\nu}$ values[27] All valence electrons were considered in the calculations, and the basis set consisted of Slater-type orbitals of double-ζ quality for C 2s and 2p as well as S 3s and 3p and of single-ζ quality for H 1s. The ionization potentials, contraction coefficients, and exponents were taken from previous work.[28]

Acknowledgments

This study was supported by the Russian Foundation for Basic Research (RFBR) (grant numbers 14-03-00119, 15-02-02723, and 15-03-20272), the Russian Academy of Sciences (program "Modern problems of low-temperature physics"), the Spanish Ministerio de Economía y Competitividad (MINECO) (grant number FIS2012-37549-C05-05), and the Generalitat de Catalunya (grant numbers 2014 SGR301 and XRQTC).

[1] M. Kurmoo, A. W. Graham, P. Day, S. J. Coles, M. B. Hursthouse, J. L. Caufield, J. Singleton, F. L. Pratt, W. Hayes, L. Ducasse, P. Guionneau, *J. Am. Chem. Soc.* **1995**, *117*, 12209–12217.

[2] L. Martin, S. S. Turner, P. Day, F. E. Mabbs, E. J. L. McInnes, *Chem. Commun.* **1997**, 1367–1368.

[3] S. S. Turner, P. Day, K. M. Abdul Malik, M. B. Hursthouse, S. J. Teat, E. J. MacLean, L. Martin, S. A. French, *Inorg. Chem.* **1999**, *38*, 3543–3549.

[4] S. Rashid, S. S. Turner, P. Day, J. A. K. Howard, P. Guionneau, E. J. L. McInnes, F. E. Mabbs, R. J. H. Clark, S. Firth, T. Biggs, *J. Mater. Chem.* **2001**, *11*, 2095–2101.
[5] S. Rashid, S. S. Turner, D. Le Pevelen, P. Day, M. E. Light, M. B. Hursthouse, S. Firth, R. J. H. Clark, *Inorg. Chem.* **2001**, *40*, 5304–5306.
[6] L. Martin, S. S. Turner, P. Day, P. Guionneau, J. A. K. Howard, D. E. Hibbs, M. E. Light, M. B. Hursthouse, M. Uruichi, K. Yakushi, *Inorg. Chem.* **2001**, *40*, 1363–1371.
[7] T. G. Prokhorova, S. S. Khasanov, L. V. Zorina, L. I. Buravov, V. A. Tkacheva, A. A. Baskakov, R. B. Morgunov, M. Gener, E. Canadell, R. P. Shibaeva, E. B. Yagubskii, *Adv. Funct. Mater.* **2003**, *13*, 403–411.
[8] E. Coronado, S. Curelli, C. Giménez-Saiz, C. J. Gómez-García, *Synth. Met.* **2005**, *154*, 245–248.
[9] L. V. Zorina, T. G. Prokhorova, S. V. Simonov, S. S. Khasanov, R. P. Shibaeva, A. I. Manakov, V. N. Zverev, L. I. Buravov, E. B. Yagubskii, *J. Exp. Theor. Phys.* **2008**, *106*, 347–354.
[10] H. Akutsu, A. Akutsu-Sato, S. S. Turner, P. Day, E. Canadell, S. Firth, R. J. N. Clark, J. Yamada, S. Nakatsuji, *Chem. Commun.* **2004**, 18–*19*.
[11] L. Martin, P. Day, H. Akutsu, J. Yamada, S. Nakatsuji, W. Clegg, R. W. Harrington, P. N. Horton, M. B. Hursthouse, P. McMillan, S. Firth, *CrystEngComm* **2007**, *9*, 865–867.
[12] A. Akutsu-Sato, H. Akutsu, J. Yamada, S. Nakatsuji, S. S. Turner, P. Day, *J. Mater. Chem.* **2007**, *17*, 2497–2499.
[13] T. G. Prokhorova, L. I. Buravov, E. B. Yagubskii, L. V. Zorina, S. S. Khasanov, S. V. Simonov, R. P. Shibaeva, A. V. Korobenko, V. N. Zverev, *CrystEngComm* **2011**, *13*, 537–545.
[14] L. V. Zorina, S. S. Khasanov, S. V. Simonov, R. P. Shibaeva, V. N. Zverev, E. Canadell, T. G. Prokhorova, E. B. Yagubskii, *CrystEngComm* **2011**, *13*, 2430–2438.
[15] L. V. Zorina, S. S. Khasanov, S. V. Simonov, R. P. Shibaeva, P. O. Bulanchuk, V. N. Zverev, E. Canadell, T. G. Prokhorova, E. B. Yagubskii, *CrystEngComm* **2012**, *14*, 460–465.
[16] A. Audouard, V. N. Laukhin, L. Brossard, T. G. Prokhorova, E. B. Yagubskii, E. Canadell, *Phys. Rev. B* **2004**, *69*, 144523-1-144523-6.
[17] E. Coronado, S. Curreli, C. Giménez-Saiz, C. J. Gómez-García, *Inorg. Chem.* **2012**, *51*, 1111–1126.
[18] T. G. Prokhorova, L. V. Zorina, S. V. Simonov, V. N. Zverev, E. Canadell, R. P. Shibaeva, E. B. Yagubskii, *CrystEngComm* **2013**, *15*, 7048–7055.
[19] I. Olejniczak, A. Frackowiak, R. Swietlik, T. G. Prokhorova, E. B. Yagubskii, *ChemPhysChem* **2013**, *14*, 3925–3935.
[20] T. G. Prokhorova, L. I. Buravov, E. B. Yagubskii, L. V. Zorina, S. V. Simonov, R. P. Shibaeva, V. N. Zverev, *Eur. J. Inorg. Chem.* **2014**, 3933–3940.
[21] J. Merino, R. H. McKenzie, *Phys. Rev. Lett.* **2001**, *87*, 237002.
[22] D. Shoenberg, *Magnetic Oscillations in Metals*, Cambridge University Press, Cambridge, UK, **1984**.
[23] M.-H. Whangbo, J. M. Williams, P. C. W. Leung, M. A. Beno, T. J. Emge, H. H. Wang, *Inorg. Chem.* **1985**, *24*, 3500–3502.
[24] *CrysAlisPro 1.171.37.34c*, Agilent Technologies.
[25] G. M. Sheldrick, *Acta Crystallogr., Sect. A* **2008**, *64*, 112–122.
[26] M.-H. Whangbo, R. J. Hoffmann, *J. Am. Chem. Soc.* **1978**, *100*, 6093–6098.
[27] J. H. Ammeter, H.-B. Bürgi, J. Thibeault, R. Hoffmann, *J. Am. Chem. Soc.* **1978**, *100*, 3686–3692.
[28] A. Pénicaud, K. Boubekeur, P. Batail, E. Canadell, P. Auban-Senzier, D. Jérome, *J. Am. Chem. Soc.* **1993**, *115*, 4101–4112.

Received: September 23, 2015
Published Online: November 9, 2015

